

A Hierarchical Approach to Study the Thermal Behavior of Protonated Water Clusters $\text{H}^+(\text{H}_2\text{O})_n$

Quoc Chinh Nguyen,[†] Yew-Soon Ong,[‡] and Jer-Lai Kuo^{†,§,*}

School of Physical and Mathematical Sciences, Nanyang Technological University, 637371, Singapore, School of Computer Engineering, Nanyang Technological University, 639798, Singapore, and Institute of Atomic and Molecular Sciences, Academia Sinica, Taipei 10617, Taiwan

Received March 16, 2009

Abstract: The energy landscape of protonated water clusters $\text{H}^+(\text{H}_2\text{O})_n$ is thoroughly explored at the first-principle level using a hierarchical search methodology. In particular, the distinct configurational isomers of OSS2 empirical potential for $n = 5–9$ are uncovered and archived systematically using an asynchronous genetic algorithm and are subsequently refined with first-principle calculations. Using the OSS2 model, quantitative agreements in the thermal properties between Monte Carlo and harmonic superposition approximation (HSA) highlighted the reliability of the latter approach for the study of small- to medium-sized protonated water clusters. From the large sets of collected isomers, finite temperature behavior of the clusters can be efficiently examined at first-principle accuracy with the use of HSA. From the results obtained, evidence of structural changes from single-ring to treelike ($n = 5–7$) and multi-ring to single-ring structures ($n = 7–9$) is observed, as expected for the empirical model. Finally, the relevance of these findings to recent experimental data is discussed.

I. Introduction

Protonated water clusters have attracted much study for a long period of time because of their important roles in ionic media and chemical reactions.^{1–16} To date, significant progress has been made in experiments^{6,7,9,12,13} and theoretical simulations.^{3–5,8,11,14–19} In the latter, one of the core focuses is studying the dynamic structural transitions to reveal the complicated thermal behavior of water clusters. Using Monte Carlo (MC) simulations, Singer and co-workers⁸ identified the topological transitions of $\text{H}^+(\text{H}_2\text{O})_8$ and $\text{H}^+(\text{H}_2\text{O})_{16}$ to treelike structures at high temperatures, using the OSS2 model.² On the other hand, Christie and Jordan,¹ with the use of the MSEVB model,²⁰ identified two sharp transitions of $\text{H}^+(\text{H}_2\text{O})_8$, whereas that of $\text{H}^+(\text{H}_2\text{O})_6$ was

devoid of sharp structures. Kuo and Klein⁴ carried out basin hopping^{18,21,22} and a parallel tempering algorithm^{23,24} to systematically examine the low-energy structures and structural transitions of $\text{H}^+(\text{H}_2\text{O})_n$ for n up to 21. In a similar work, James and Wales²⁵ employed a modified empirical valence bond potential to study the properties of selected small- to medium-sized clusters. With the advance of computation power and methodology, several studies have been conducted in an attempt to study water clusters at ab initio levels.^{15,16,26–28} Iyengar and co-workers proposed the ab initio atom-centered density matrix propagation method to investigate systematically the structures, dynamics, and vibrational properties of $\text{H}^+(\text{H}_2\text{O})_n$ for the magic size of $n = 21$,^{15,16} as well as other systems.²⁹ Recently, Nakayama et al.²⁶ considered the use of an approximate potential to speed up the ab initio MC simulation on small protonated water clusters ($\text{H}^+(\text{H}_2\text{O})_{n=1,2}$).

Most of the existing theoretical simulations have engaged either molecular dynamics (MD) or MC-based algorithms in predicting the structural transitions of $\text{H}^+(\text{H}_2\text{O})_n$.^{1,4,8,17} Even though some techniques such as J-walk^{25,26} and parallel

* Corresponding author fax: + 886-223620200, e-mail: jlk@pub.iams.sinica.edu.tw.

[†] School of Physical and Mathematical Sciences, Nanyang Technological University.

[‡] School of Computer Engineering, Nanyang Technological University.

[§] Academia Sinica.

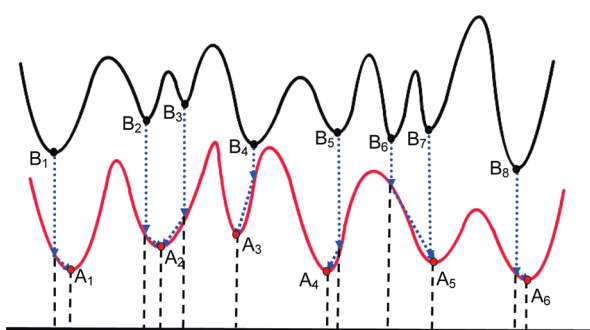


Figure 1. Sketch of hierarchical approach. A_i and B_i refer to the local minima of the empirical model (black curve) and ab initio calculations (red curve), respectively. The local minima B_i have been identified with the genetic algorithm to serve as appropriate starting points for further refinement or locally optimized using the ab initio calculations to arrive at the respective A_i .

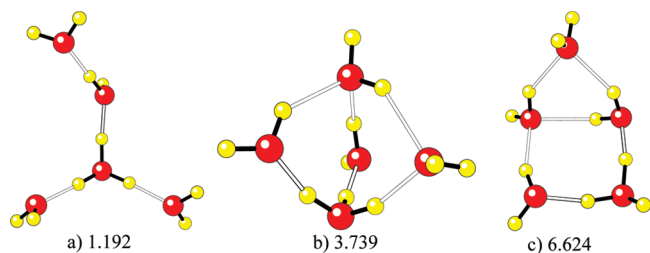


Figure 2. Several new isomers of $\text{H}^+(\text{H}_2\text{O})_5$. The numbers are denoted as relative energies in kcal/mol.

tempering are established as useful for resolving the issue of quasi-ergodicity, they remain to be plagued with problems of slow convergence, high energy barrier crossing, and poor sampling of the potential energy landscape, especially in large-scale or large-sized systems. An alternative approach to MD and MC is superposition approximation (SA), where the observed quantities of the system are approximated from a statistical set of basins instead of performing sampling and averaging of the entire potential energy surface (PES). To date, SA has been used widely in a variety of systems, from liquids to solids, glasses, clusters, and so forth. It was first considered by Stillinger et al. for studying hidden structures in liquids³⁰ and subsequently also liquid–solid transitions.³¹ Wales examined the coexistence of solid-like and liquid-like forms in a finite atomic cluster, with harmonic approximation employed in SA for the first time.³² Calvo et al.³³ also used SA to calculate the physical and chemical properties of several atomic clusters and highlighted the close agreement between SA and MC simulations. Generally, SA is established to yield higher efficiency than conventional MC simulations in predicting thermal properties,^{33–35} thus making SA feasible and practical for studying the thermodynamics of molecular systems at the quantum chemistry level. Since the accuracy and success of SA depends strongly on how well the PES is explored and how many isomers are taken into account for the approximation, a sampling algorithm for the effective and efficient discovery of true distinct isomers is crucial. Note that this is not a trivial task due to the large numbers of isomers that exist and the high computational costs of ab initio calculations.

Recently, Ohno and co-workers^{5,11} proposed the “anharmonic downward distortion following” (ADD) algorithm, a full first-principle-based approach, to explore the PES and then examined the thermodynamics of $\text{H}^+(\text{H}_2\text{O})_n$ for n up to 7 via harmonic superposition approximation (HSA). The sets of 9, 24, and 131 isomers collected for $n = 5, 6$, and 7, respectively, at B3LYP/6-31+G** level were reasonably large. However, the requirement on second-order derivative calculations and the serial searching regime limits the ADD from sampling widely for high-energy isomers on the quantum chemistry PES, especially for larger-sized systems.

In the present work, instead of a complete reliance on ab initio calculations, we employ a hierarchical methodology with the OSS2 model employed as a prescreening process to construct the archive of potential distinct isomers for $n = 5–9$ to be subsequently examined and refined by first-principles calculations at the B3LYP/6-31+G* level. The synergy between the empirical model and first-principles method permits extensive and efficient exploration of the PES, dealing with large-sized systems (up to $n = 9$), and studying the systems at multiple distinctive levels of theory simultaneously. To deal with the issue of exponential growth of the number of isomers, a parallel asynchronous genetic algorithm is deployed for the searching and archiving of distinct configurational isomers in $\text{H}^+(\text{H}_2\text{O})_n$. The archive of isomers is then analyzed to investigate the thermodynamic properties and structural transitions of $\text{H}^+(\text{H}_2\text{O})_n$, $n = 5–10$, for both the OSS2 model and ab initio calculations. From our obtained results, HSA is shown to be reliable in small-sized systems since it reproduces well the feature of heat capacity curves and structural transition of $\text{H}^+(\text{H}_2\text{O})_n$ in MC simulations of the OSS2 model. The structural transition trends of protonated water clusters in ab initio calculations also revealed close agreement with that of the OSS2 model. The vibrational spectra are derived from the results of HSA and compared with recent experimental study. The details of our computational methodology are described in section II, followed by the results and discussion in section III.

II. Methodology

1. A Hierarchical Approach for Exploration of PES. Our hierarchical approach has been previously explored and applied to the study of pure water clusters.³⁶ Here, we briefly discuss the main ideas of our methodology as depicted in Figure 1. Instead of searching directly on the PES of ab initio calculations (red curve), which is computationally very expensive, we locate the isomers, denoted here as B_i , of the empirical model (black curve), which serves as a “prescreening” stage. All distinct isomers B_i are subsequently refined to the nearest isomers A_i via ab initio optimizations. The low computational cost of the empirical model allows possible extensive coverage and exploration of the PES for unique isomers. To speed up the entire isomer search process, the ab initio refinements representing the most time-consuming tasks are parallelized on multiple computed clusters.

2. Empirical Models. In this work, the OSS2 model is chosen as the first level of exploration. OSS2 is one of three versions of the OSS family developed by Ojamäe and co-

| | W5+ | W6+ | W7+ | W8+ | W9+ |
|------|---------|----------|----------|----------|----------|
| I | | | | | |
| | -99.184 | -113.854 | -129.765 | -145.381 | -159.635 |
| II | | | | | |
| | -97.981 | -113.834 | -129.379 | -144.657 | -159.127 |
| III | | | | | |
| | -97.920 | -113.602 | -129.365 | -144.511 | -158.400 |
| IV | | | | | |
| | -96.786 | -113.421 | -129.244 | -144.416 | -158.398 |
| V | | | | | |
| | -96.009 | -113.321 | -128.235 | -144.290 | -158.237 |
| VI | | | | | |
| | -95.445 | -113.293 | -128.225 | -144.116 | -158.105 |
| VII | | | | | |
| | -95.357 | -113.247 | -128.184 | -144.109 | -158.021 |
| VIII | | | | | |
| | -95.275 | -113.211 | -128.173 | -143.730 | -157.951 |
| IX | | | | | |
| | -94.998 | -113.132 | -128.172 | -143.558 | -157.920 |
| X | | | | | |
| | -94.807 | -112.977 | -128.166 | -143.550 | -157.769 |

Figure 3. The 10 lowest-energetic isomers of $\text{H}^+(\text{H}_2\text{O})_n$, $n = 5-9$, found in B3LYP/6-31+G*, sorted by increasing order of binding energies (in kcal/mol).

workers² to simulate water as a participant in ionic chemistry. It was established from the interaction between polarizable O²⁻ anions and protons, with pairwise and three-body terms, and is suitable for studying H⁺(H₂O)_n system since it permits the disassociation of water molecules. The potential was parametrized by fitting to ab initio MP2 calculations, and it can reproduce well the structures and binding energies of small-sized protonated water clusters, including neutral ones. For details on the functional forms and thermodynamic simulations of OSS2, the reader is referred to refs 2 and 4.

3. Asynchronous Genetic Algorithm. Archiving isomers is a nontrivial task due to the exponentially increasing number of isomers with increasing cluster sizes. To deal with this issue, we conducted a steady-state genetic algorithm (GA) with an asynchronous scheme for locating isomers, which we have previously used to study the PES of water clusters.³⁶

The basic workflow of our GA is outlined as follows: After initialization, parent structures are selected from the population according to their ranks and undergo the genetic operators (crossover and/or mutation) to generate new offspring, which are sent to a slave node for local optimization. The locally optimized structure is then sent back to the master node, which is then updated into the GA population with the spirit of Lamarckian Learning^{37,38} and also archived for further analysis. This entire process repeats until a maximum number of iterations is reached. More specifically, the search algorithm is commonly known as a memetic algorithm, hybrid evolutionary algorithm, Lamarckian evolutionary algorithm, cultural algorithm, or genetic local search.³⁹

Throughout the archiving process, a significant number of structures, including the low-energetic isomers, may be archived more than once. These duplicate structures not only

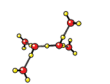
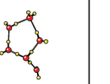
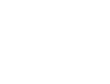
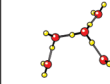
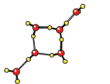
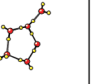
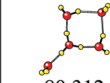
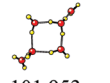
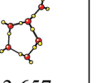
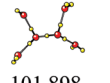
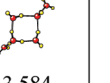
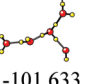
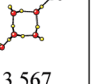
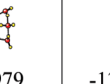
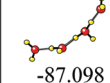
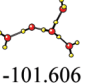
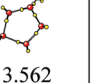
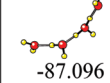
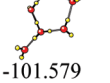
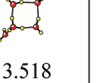
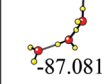
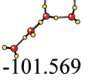
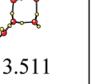
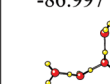
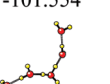
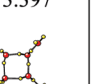
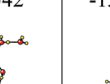
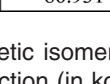
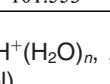
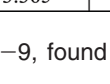
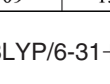
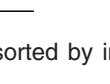
| | W5+ | W6+ | W7+ | W8+ | W9+ |
|------|---|---|---|--|---|
| I |  |  |  |  |  |
| | -89.645 | -102.271 | -114.160 | -125.739 | -136.998 |
| II |  |  |  |  |  |
| | -89.354 | -101.967 | -113.689 | -125.091 | -136.835 |
| III |  |  |  |  |  |
| | -89.312 | -101.953 | -113.657 | -125.070 | -136.714 |
| IV |  |  |  |  |  |
| | -87.334 | -101.898 | -113.584 | -125.047 | -136.538 |
| V |  |  |  |  |  |
| | -87.123 | -101.633 | -113.567 | -124.979 | -136.220 |
| VI |  |  |  |  |  |
| | -87.098 | -101.606 | -113.562 | -124.881 | -136.216 |
| VII |  |  |  |  |  |
| | -87.096 | -101.579 | -113.518 | -124.747 | -135.971 |
| VIII |  |  |  |  |  |
| | -87.081 | -101.569 | -113.511 | -124.617 | -135.943 |
| IX |  |  |  |  |  |
| | -86.997 | -101.554 | -113.397 | -124.542 | -135.801 |
| X |  |  |  |  |  |
| | -86.931 | -101.553 | -113.365 | -124.509 | -135.795 |

Figure 4. The 10 lowest-energetic isomers of $\text{H}^+(\text{H}_2\text{O})_n$, $n = 5-9$, found in B3LYP/6-31+G*, sorted by increasing order of binding energies with ZPE correction (in kcal/mol).

enlarge the archive unnecessarily but also make the simulation results unreliable since the contribution by some isomers could be artificially amplified. To ensure that only unique structures are archived, the ultrafast structure recognition (USR) algorithm⁴⁰ is used to sieve out potential duplicate structures. The similarity of two structures is computed and represented by an index of values ranging from 0 to 1. A value of 0 indicates that two structures are totally dissimilar, whereas the other extreme represent a perfect match. In our study, a newly discovered structure is deemed as a duplicate if the similarity index to existing structures in the archive exceeds a threshold of 0.96.

4. Ab Initio Calculation. All archived distinct isomers of the OSS2 model then undergo geometrical optimization using Becke's three-parameter hybrid method⁴¹ with the Lee, Yang, and Parr (B3LYP) functional⁴² and the 6-31+G* basis set. The convergence criteria are defined as a root-mean

square and a maximum component of gradient lower than 0.0003 and 0.00045 hartree/Å, respectively. To ensure that the optimized structures are true isomers, vibration analysis is subsequently performed, and only those having nonimaginary frequencies are accepted for harmonic superposition approximation. Note that all calculations have been completed using the Gaussian 03 package.⁴³

III. Results and Discussions

1. Isomers of Protonated Water Clusters. It is worth highlighting that our GA has reproduced successfully all of the most stable structures of $\text{H}^+(\text{H}_2\text{O})_n$, $n = 5-9$, that were found by the basin-hopping algorithm reported in previous related works.⁴ In addition to that, we have uncovered and archived large numbers of distinct isomers which are summarized in Table 1. Since a threshold value of 0.96 was

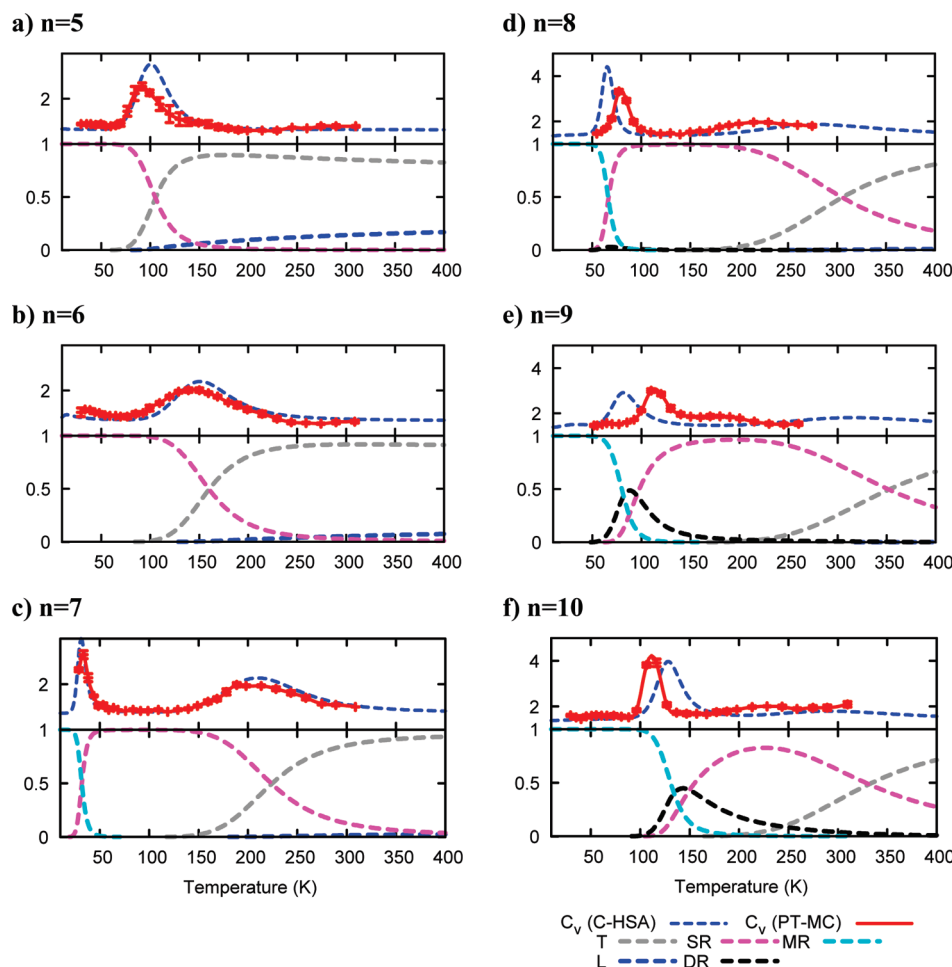


Figure 5. Canonical heat capacity C_v (upper panel) and population (lower panel) of five topologies for $H^+(H_2O)_n$, $n = 5–10$, that is, multi-ring (MR), double-ring (DR), single-ring (SR), linear (L), and tree-like (T), calculated using C-HSA with the OSS2 model. Solid-red and dashed-blue lines in the upper panels represent heat capacity curves from a previous parallel tempering Monte Carlo (PT-MC) simulation⁴ and our C-HSA, respectively. For the sake of brevity, the heat capacity is plotted with a dimensionless unit (Nk_B).

employed in the USR technique to remove duplicate isomers automatically, an overelimination of unique isomers may happen. The resultant archive therefore may not represent the complete set of isomers on the PES. However, from our results, the number of distinct isomers, N_{isomers} , is observed to increase exponentially with the number of atoms, N , in the range of $n = 5–9$, as expected in both theoretical and numerical studies.^{34,44} N_{isomers} can be approximated as $A \times \exp(\alpha N)$, where both A and α are constants depending on the system considered. From the database of Lennard-Jones clusters, A and α have been approximated as 0.00397 and 0.9897, respectively, for $N \leq 16$.^{45,46} In the present work, A and α are approximated as 0.5849 and 0.3918, respectively. The significantly larger A for $H^+(H_2O)_n$ might arise from the fact that the water cluster system is less symmetric than atomic counterparts. This explains the larger number of isomers identified in the small-sized water clusters and, hence, a larger “ A ” value. Thus, A might represent the measure of asymmetry in the system. In contrast, the smaller value of α of the water cluster system would imply its smaller degree of freedom due to the bonds.

The uncovered sets of archived OSS2 isomers subsequently serve as input structures that are optimized at the

B3LYP/6-31+G* level. At the end of each successful optimization, the local optima at B3LYP/6-31+G* undergo vibrational analysis, which is performed to retrieve the vibrational frequencies. For $H^+(H_2O)_5$, $H^+(H_2O)_6$, and $H^+(H_2O)_7$, a total of 21, 135, and 707 isomers have been uncovered and archived, respectively. For $H^+(H_2O)_8$ and $H^+(H_2O)_9$, because the numbers of isomers found using the OSS2 model are large, a stricter similarity threshold of 0.85 is used to filter out a greater number of potentially duplicated OSS2 isomers before undergoing DFT optimization. On the basis of the given criterion, resultant sets of 422 and 877 isomers for $H^+(H_2O)_8$ and $H^+(H_2O)_9$, respectively, have been identified. In comparison to other recent works reported in the literature from similar studies,^{5,11} the archives represent the largest sets of isomers reported at the quantum chemistry level to date. For instance, several isomers of $H^+(H_2O)_5$ that are missing in the recent reported work¹¹ are depicted in Figure 2.

The 10 lowest-energetic isomers of each cluster size have been sorted according to their binding energies and are depicted in Figure 3. As observed, the ground-state structures of both $H^+(H_2O)_5$ and $H^+(H_2O)_6$ belong to the family of four-membered rings, as observed in the OSS2 model. In

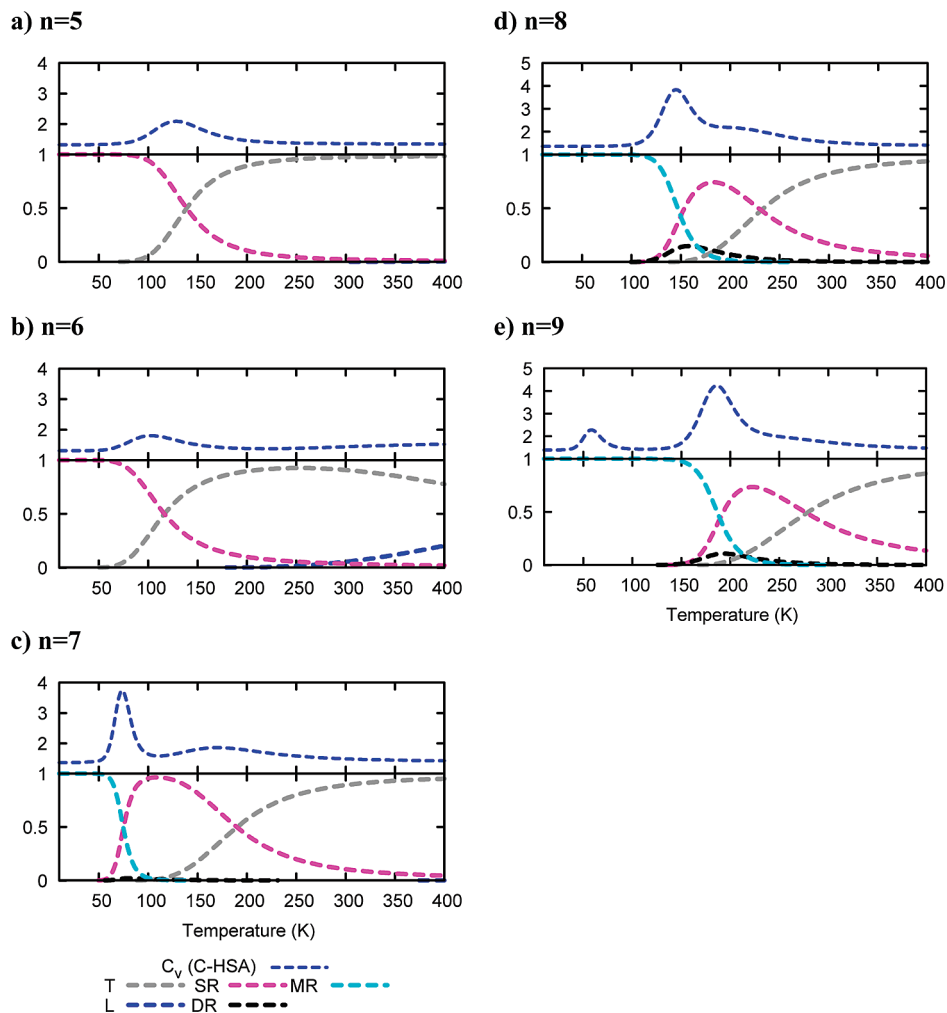


Figure 6. Canonical heat capacity C_v (upper panel) and population (lower panel) of five topologies of $H^+(H_2O)_n$, $n = 5–9$, calculated using C-HSA with B3LYP/6-31+G* calculation. The full details have been described in Figure 5.

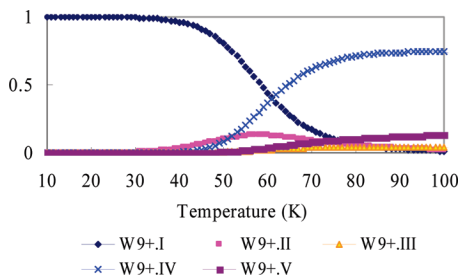


Figure 7. Population plot of the five lowest-energetic isomers of $H^+(H_2O)_9$ calculated using C-HSA with B3LYP/6-31+G* isomers. The transition from the lowest-energetic isomer (W9+.I) to the next lowest-energetic ones resulted in the first heat capacity peak of Figure 6e.

$H^+(H_2O)_5$, several other families of isomer shapes are also found to exist, as depicted in Figure 3. These include five-membered ring isomers and tree-like or cage isomers which are well separated at the energy level (~ 1 kcal/mol). On the other hand, the family of four-membered ring isomers is observed to dominate, with near iso-energetic values at a small energy gap of less than 0.2 kcal/mol. For $H^+(H_2O)_7$ and large-sized clusters, the structures tend to be more compact, and all ground-state and low-energetic structures are of multi-ring shapes. The cubic isomers of $H^+(H_2O)_8$

are also relatively stable with a small energy gap of approximately 0.9 kcal/mol to the ground-state counterpart. Note that this is in line with the observation reported by James and Wales²⁵ where the lowest cubic-like minimum of the modified MSEVB potential is approximately 0.8 kcal/mol higher than the most stable structure.

Figure 4 depicts the structures of $H^+(H_2O)_n$ sorted according to the energy after zero-point energy correction. It is worth noting that the resultant structures of all sizes are observed to be more open. For $H^+(H_2O)_5$ and $H^+(H_2O)_6$, tree-like isomers have the lowest energy instead of single-ring isomers, whereas for $H^+(H_2O)_7$, the single-ring structures dominate. For $H^+(H_2O)_8$ and $H^+(H_2O)_9$, the lowest-energetic isomers are no longer cages, and few single-ring isomers are found. Besides the fact that open isomers are more favored, they are also more iso-energetic since the energy gaps between them are smaller (<1 kcal/mol) than those without zero-point energy.

2. Thermodynamic Transitions. a. Harmonic Superposition Approximation. HSA represents an effective approach for acquiring the diverse physical properties of a system from a collection of isomers instead of directly exploring the potential energy landscape. In HSA, each local minimum is treated as a harmonic and infinite basin, which

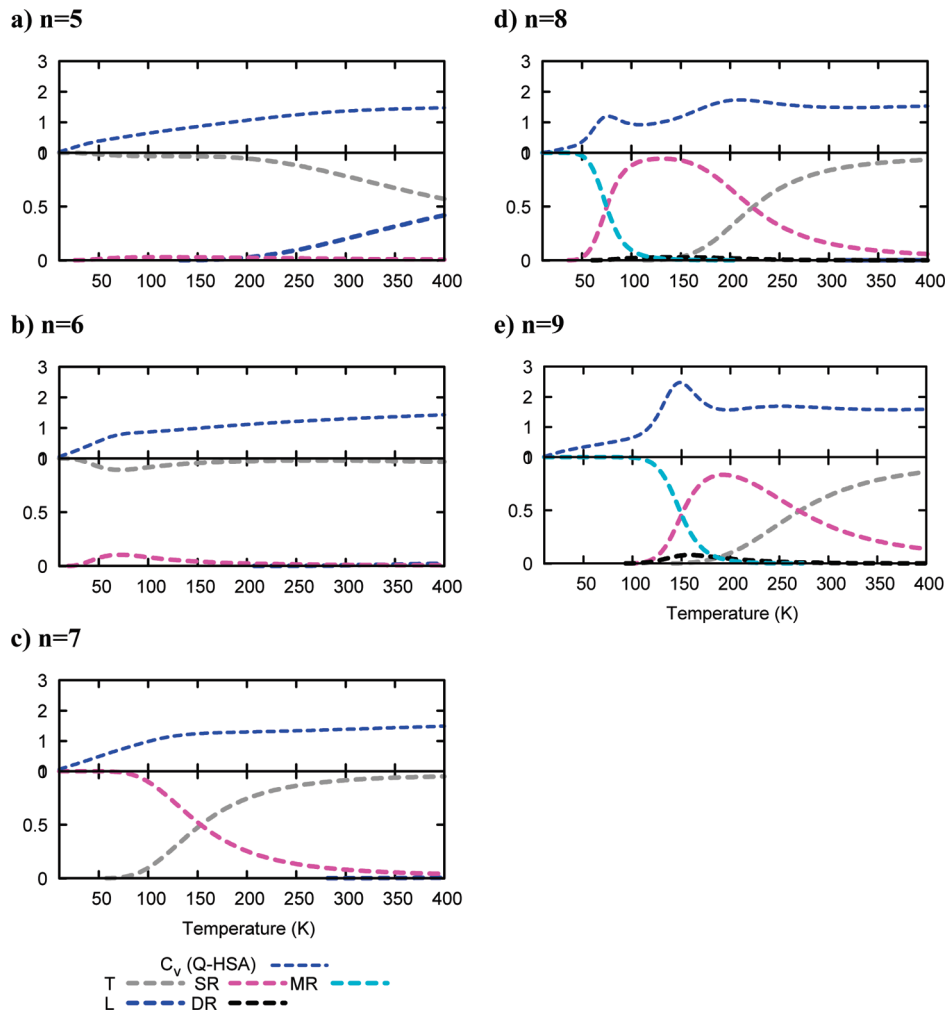


Figure 8. Canonical heat capacity C_v (upper panel) and population (lower panel) of five topologies of $\text{H}^+(\text{H}_2\text{O})_n$, $n = 5-9$, calculated using quantum HSA (Q-HSA) with B3LYP/6-31+G* calculation. The full details have been described in Figure 5.

is characterized only by its vibrational frequencies and relative energy. From that, observable quantities are subsequently calculated by summing up the contributions of all isomers.

The total partition function $Z(\beta)$ of an N -atom system at temperature T is given by

$$Z(\beta) = \sum_a n_a Z_a(\beta)$$

where $\beta = 1/(k_B T)$ and k_B is the Boltzmann constant. The degeneracy factors n_a in the case of $\text{H}^+(\text{H}_2\text{O})_n$ (consisting of two kinds of atomic elements, O and H) are derived as $2N_{\text{O}}!N_{\text{H}}!/m_i$, where m_i is the point group order of symmetry. In classical superposition theory (classical harmonic superposition approximation, C-HSA), the harmonic approximation associated with local minima a , $Z_a(\beta)$, is given by^{33,34}

$$Z_a^C(\beta) = \exp(-\beta E_a)/(\beta \hbar \overline{\omega}_a)^{N_f}$$

where $\overline{\omega}_a = (\prod_{f=1}^{N_f} \omega_{af})^{1/N_f}$ denotes the mean geometrical vibration frequencies of local minimum a and $N_f = 3N - 6$, representing the number of normal modes. In quantum superposition theory (quantum harmonic superposition approximation, Q-HSA), where the contributions of the vibra-

tion modes are treated in quantum mechanical footing, $Z_a(\beta)$ assumes the following form:

$$Z_a^Q(\beta) = \exp(-\beta E_a) \prod_a \frac{\exp(-\beta \hbar \omega_{af}/2)}{1 - \exp(-\beta \hbar \omega_{af})}$$

To observe the structural transformations, isomers of $\text{H}^+(\text{H}_2\text{O})_n$ are classified into five categories of topological families, namely, multi-ring, double-ring, single-ring, tree-like, and linear. The population or the canonical probability of the system to fall under topology A is calculated as $P_A(T) = (\sum_{a \in A} Z_a(\beta))/(Z(\beta))$. Other observables including specific heat capacity and free energy can also be easily derived on the basis of the details available in refs 34 and 46.

b. Comparison with Parallel Tempering Monte Carlo (PTMC) Simulation. In Figure 5, the temperature dependences of heat capacity and the populations of five topological families obtained for $\text{H}^+(\text{H}_2\text{O})_n$, $n = 5-10$, are depicted. For possible comparison, the heat capacity trends obtained by the parallel tempering Monte Carlo (PTMC) simulations as reported in ref 4 are reproduced in Figure 5 with the use of cubic-spline smoothing.

From Figure 5, HSA is observed to reproduce the transition peaks of the heat capacity trace well, on both sizes 5 and 6. Both methods predicted similar transition temperatures in

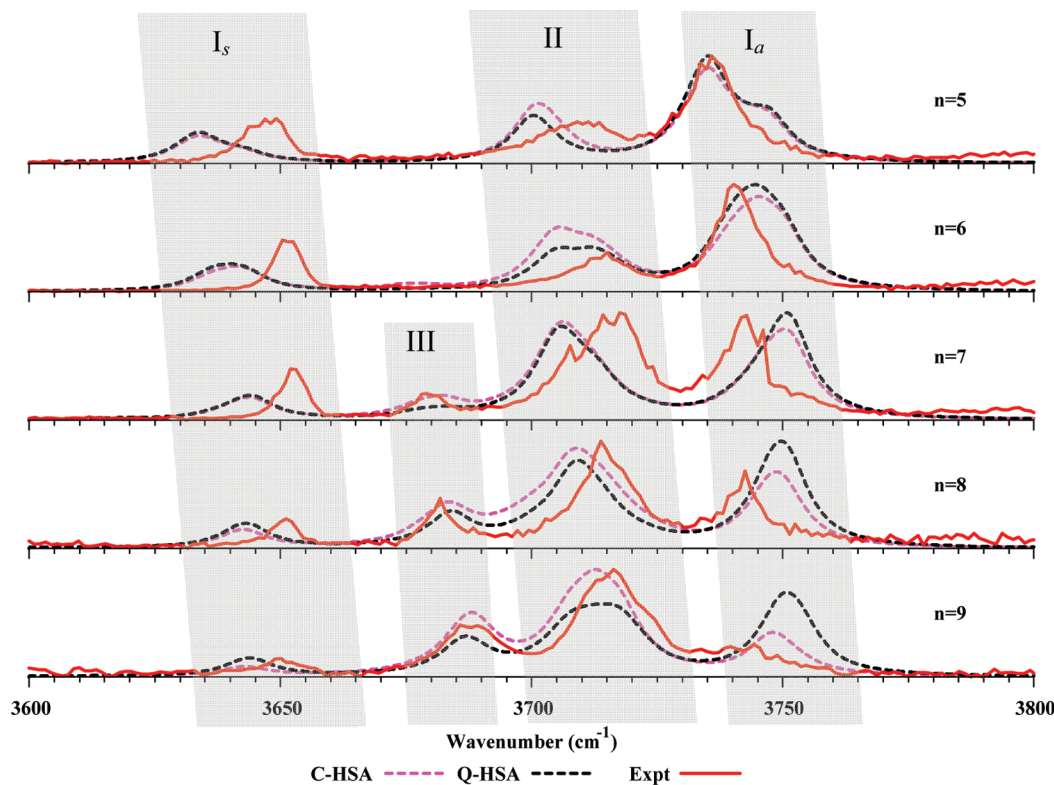


Figure 9. Vibrational spectra of free OH-stretching bands for $\text{H}^+(\text{H}_2\text{O})_n$, $n = 5–9$, calculated using classical (C-HSA) and quantum (Q-HSA) theories of harmonic superposition approximation. The experimental results of ref 7 are also plotted as a solid-red curve for the purpose of comparison.

Table 1. Number of Distinct Isomers in OSS2 Potential for $\text{H}^+(\text{H}_2\text{O})_n$, $n = 5–10$

| n | OSS2 |
|-----|-------|
| 5 | 218 |
| 6 | 1192 |
| 7 | 4700 |
| 8 | 11820 |
| 9 | 24693 |
| 10 | 32469 |

the proximity of 100 K and 150 K for $\text{H}^+(\text{H}_2\text{O})_5$ and $\text{H}^+(\text{H}_2\text{O})_6$, respectively. An analysis of the populations of topologies also indicated the domination by single-ring structures dominating at low temperatures and their transformations to tree-like forms. On the other hand, linear structures significantly populating the archive appear only at high temperatures with low probability. A similar observation was also recognized in PTMC simulations.

For $n \geq 7$, where multi-ring structures pose as the most stable, there are two maxima corresponding to two structural transitions: an exceptionally sharp peak for the rapid changes of multi-ring to single-ring structures and a broad and shorter peak for the gradual changes of single-ring to tree-like structures. In the case of $\text{H}^+(\text{H}_2\text{O})_7$, the transition temperatures predicted by HSA are again in close agreement with those obtained by PTMC; that is, a significant rise at a low temperature of 40 K and a bump at a higher temperature of ~ 230 K is observed in both. For $\text{H}^+(\text{H}_2\text{O})_8$, HSA produces slight difference in the prediction of transition temperatures; that is, the first peak (60 K) is lower in PTMC (70 K), as expected, while the second peak shifts to a higher temper-

ature. Nevertheless, the overall feature and trend of the population and heat capacity obtained using HSA correlates well with that using PTMC.

For sizes 9 and 10, the transition temperatures become more difficult to predict accurately since both PTMC and HSA fail to converge well. Note that the increase in transition temperatures due to cluster size in HSA matches that predicted by PTMC previously. These results also revealed transitions from single-ring to tree-like structures happening for all of the cluster sizes investigated and the transition temperature shifting higher with growing cluster size. It is also worth noting the absence of double-ring structures for $n = 5, 6, 7$, and 8 in the population plots, even though double-ring structures significantly populate the archive.

In most cases, except the first peaks of $\text{H}^+(\text{H}_2\text{O})_8$ and $\text{H}^+(\text{H}_2\text{O})_9$, HSA seems to have overestimated the transition peak when compared to PTMC, and the shapes of these peaks are noted to be somewhat sharper. However, the overestimation is relatively small and regarded as acceptable for $n \leq 8$, although there is a slight increase for $n \geq 9$. We believe one of the core reasons is related to the underestimations of contributions made by the high-energy local minima, since our exploration of the PES for OSS2 using GA has placed greater emphasis on the low-energy region than the high-energy counterpart. Hence, the entropy of high-energy topologies in the form of tree and linear shapes has generally been underestimated. The resultant impact is a broadening and shifting of the high-temperature transition peak to higher temperatures, while it is a sharpening and swing in the low-temperature transition peak to lower temperatures.

c. DFT Calculation. Employing conventional Monte Carlo methods to simulate thermodynamics in DFT calculations is impractical, even for small-sized systems, due to the high computational cost involved. The use of HSA, on the other hand, serves to be more appropriate due to its higher efficiency compared to conventional MC approaches. Furthermore, HSA has also been shown to yield good quantitative agreement with Monte Carlo simulation on small-sized systems, as demonstrated in the previous sections for the OSS2 model. In what follows, we discuss the use of HSA to study protonated water clusters with DFT calculation in both classical (C-HSA) and quantum (Q-HSA) theory.

i. In Classical Theory. Using the archive of local minima, we applied classical HSA to simulate the thermodynamic transitions. It can be observed in Figure 6 that the heat capacity trend obtained using DFT calculations correlates well with those produced on the basis of the OSS2 model for $n = 5–7$. In the cases of $\text{H}^+(\text{H}_2\text{O})_5$ and $\text{H}^+(\text{H}_2\text{O})_6$, a small maximum representing the transition from single-ring to tree-like structures can be observed. The DFT results show a higher transition temperature with a phase change that is more gradual, as reflected by a flat and shorter peak. For $\text{H}^+(\text{H}_2\text{O})_7$ and $\text{H}^+(\text{H}_2\text{O})_8$, on the other hand, the two transition points found on DFT are similar to those of OSS2, except with the first occurring at a higher temperature than that in the OSS2 model and the other at a lower temperature. Further, the two peaks of $\text{H}^+(\text{H}_2\text{O})_8$ are relatively close and appear to merge as single peak in the case of $\text{H}^+(\text{H}_2\text{O})_9$. Note also the small peak in the heat capacity trend of $\text{H}^+(\text{H}_2\text{O})_9$ at ~ 60 K, which corresponds to the transition of the lowest-energetic isomer (denoted as W9+.I in Figure 3) to the second (W9+.II), third (W9+.III), and fourth (W9+.IV) lowest energetic isomers, as depicted in Figure 7. Double-ring isomers appear to start from $\text{H}^+(\text{H}_2\text{O})_9$, but only survive within a small range of temperature (around 150 K). The overall trend of the structural transitions agrees very well with the OSS2 model, except on the precise positions of the transition temperatures. The size dependency of structural transitions is also consistent with the OSS2 model. The shift to higher temperatures from single-ring to tree-like structures with increasing size is also observed for $T_c = 120, 135, 170, 240$, and 275 K for $\text{H}^+(\text{H}_2\text{O})_n$, $n = 5, 6, 7, 8$, and 9, respectively.

ii. In Quantum Theory. The key difference between quantum HSA and its classical counterpart lies in the involvement of zero-point energy. As mentioned in section III.2.c.i, the inclusion of zero-point energy changes the relative stability of the structures, making open structures such as tree-like and linear forms more favorable. In this section, we discuss their impacts on thermodynamic properties.

The population and canonical heat capacity plots of quantum HSA are depicted in Figure 8. For $\text{H}^+(\text{H}_2\text{O})_5$ and $\text{H}^+(\text{H}_2\text{O})_6$, tree-like structures predominate the population in the range of 0–400 K instead of single-ring forms. As a result, there is almost no structural transition, as reflected in the heat capacity plots. For $\text{H}^+(\text{H}_2\text{O})_7$, only one maximum of the transformation from single-ring to tree-like structures arises at around 150 K, and in contrast to classical HSA, there is zero contribution by multi-ring structures. It is worth

noting that the observations made are consistent with the recent work reported by Luo and Ohno.¹¹

For $\text{H}^+(\text{H}_2\text{O})_8$ and $\text{H}^+(\text{H}_2\text{O})_9$, the transition characteristics are similar to classical HSA. Two main transitions, namely, from multi-ring to single-ring and from single-ring to tree-like structures, displayed small contributions of double-ring structures at around 150 K. In addition, the transitions seem to occur at lower temperatures than classical HSA. This makes sense since the zero-point energy correction has the effect of decreasing the entropy of compact structures. As explained earlier in section III.2.b, this causes the shift in transitions to lower temperatures.

3. Vibrational Spectra in Free OH-Stretching Region. From the results of vibrational analysis, the IR spectrum $I_a(\omega)$ of each isomer a is approximated using the Lorentz line shape. The total IR spectrum $I_{\text{total}}(\omega, T)$ is then calculated as the weighted sum of $I_a(\omega)$ with the canonical probability $p_a(T)$ of each isomer a derived from thermodynamic simulations, which is given by

$$I_{\text{total}}(\omega, T) = \sum_a I_a(\omega) p_a(\omega, T)$$

In Figure 9, the IR spectra calculated using both C-HSA and Q-HSA in the free OH-stretching region are plotted together with the experimental results, which are reproduced from the work of Lin and co-workers.⁷ For consistency and fair comparison, the spectra are simulated at temperature $T = 170$ K, which lies within the range of cluster temperatures used in Lin and co-workers' work,⁷ as deduced from the Arrhenius equation.⁴⁷ In addition, several relevant works^{5,11} have typically considered a temperature of 170 K in their investigations on protonated water clusters. Note that all calculated frequencies are also scaled by a factor of 0.973, as suggested in a recent related work.⁴⁸

Four groups of peaks in the free-OH stretching region are highlighted in Figure 9, namely, symmetric free-OH, asymmetric free-OH of one-coordinate H_2O , free-OH of three-coordinate H_2O , and free-OH of two-coordinate H_2O , which are denoted as I_s, I_a, II, and III, respectively. As inferred from the figure, the theoretical spectra derived from both C-HSA and Q-HSA also indicated size dependency, as observed in experimental research. The intensities of peaks I_s (around 3650 cm^{-1}) and peaks I_a (around 3750 cm^{-1}) decrease with increasing cluster size. Nevertheless, our results underestimated the relative decrease of peaks I_a, especially for $\text{H}^+(\text{H}_2\text{O})_9$, with C-HSA showing better approximation accuracy than Q-HSA, even though the prediction is generally higher than in experimental research. The calculated spectra also agree with the experimental observation that peaks II associated to the free-OH stretching band of three-coordinate H_2O appeared at $n = 7$, and the intensity continues to rise consistently when n increases. As mentioned in the study of Lin et al.,⁷ this trend can serve as evidence of a structural transition to ring isomers. Note that this agrees with the thermodynamic results discussed in the previous section where the ring isomers started to predominate the population at $n = 7$. The blue-shift of the whole free-OH stretching bands witnessed in the experiment is also observed in our calculated spectra.

IV. Conclusions

In this work, we have considered a hierarchical approach to thoroughly explore the PES of $\text{H}^+(\text{H}_2\text{O})_n$, $n = 5-10$, with the OSS2 potential model and $n = 5-9$ at the B3LYP/6-31+G* level. The distinct isomer set uncovered using our hierarchical methodology is the largest-ever archive found to date. The archive is subsequently used for the investigating the thermodynamic and structural transitions of $\text{H}^+(\text{H}_2\text{O})_n$ at two theoretical levels, namely, the OSS2 model and the B3LYP/6-31+G* level using the harmonic superposition approximation approach. In comparison with the PTMC simulation involving the OSS2 model, our results revealed good quantitative agreement between HSA and PTMC. The consistency with PTMC results in structural transition and features of the capacity curve are good indications of HSA's reliability. Further, the simulations with the ab initio method also revealed the size dependency of $\text{H}^+(\text{H}_2\text{O})_n$ in both thermal behavior and vibrational spectra. The calculated vibrational spectra in the free-OH stretching band when compared to recent experimental results also arrived at good agreement.

Acknowledgment. This research is financially supported by Academia Sinica, Nanyang Technological University, and the National Science Council (NSC98-2113-M-001-029-MY3) of Taiwan.

References

- (1) Christie, R. A.; Jordan, K. D. *J. Phys. Chem. B* **2002**, *106*, 8376.
- (2) Ojamäe, L.; Shavitt, I.; Singer, S. J. *J. Chem. Phys.* **1998**, *109*, 5547.
- (3) Svanberg, M.; Pettersson, J. B. C. *J. Phys. Chem. A* **1998**, *102*, 1865.
- (4) Kuo, J. L.; Klein, M. L. *J. Chem. Phys.* **2005**, *122*, 1.
- (5) Luo, Y.; Maeda, S.; Ohno, K. *J. Phys. Chem. A* **2007**, *111*, 10732.
- (6) Jiang, J. C.; Wang, Y. S.; Chang, H. C.; Lin, S. H.; Lee, Y. T.; Niedner-Schatteburg, G.; Chang, H. C. *J. Am. Chem. Soc.* **2000**, *122*, 1398.
- (7) Lin, C. K.; Wu, C. C.; Wang, Y. S.; Lee, Y. T.; Chang, H. C.; Kuo, J. L.; Klein, M. L. *Phys. Chem. Chem. Phys.* **2005**, *7*, 938.
- (8) Singer, S. J.; McDonald, S.; Ojamäe, L. *J. Chem. Phys.* **2000**, *112*, 710.
- (9) Wu, C. C.; Lin, C. K.; Chang, H. C.; Jiang, J. C.; Kuo, J. L.; Klein, M. L. *J. Chem. Phys.* **2005**, *122*.
- (10) Wu, C. C.; Chaudhuri, C.; Jiang, J. C.; Lee, Y. T.; Chang, H. C. *J. Chin. Chem. Soc.* **2002**, *49*, 769.
- (11) Luo, Y.; Ohno, S. M. K. *J. Comput. Chem.* **2008**, *30*, 952.
- (12) Headrick, J. M.; Diken, E. G.; Walters, R. S.; Hammer, N. I.; Christie, R. A.; Cui, J.; Myshakin, E. M.; Duncan, M. A.; Johnson, M. A.; Jordan, K. D. *Science* **2005**, *308*, 1765.
- (13) Miyazaki, M.; Fujii, A.; Ebata, T.; Mikami, N. *Science* **2004**, *304*, 1134.
- (14) Tuckerman, M.; Laasonen, K.; Sprik, M.; Parrinello, M. *J. Chem. Phys.* **1995**, *103*, 150.
- (15) Iyengar, S. S. *J. Chem. Phys.* **2007**, *126*, 216101.
- (16) Iyengar, S. S.; Petersen, M. K.; Day, T. J.; Burnham, C. J.; Teige, V. E.; Voth, G. A. *J. Chem. Phys.* **2005**, *123*, 084309.
- (17) Mella, M.; Kuo, J.-L.; Clary, D. C.; Klein, M. L. *Phys. Chem. Chem. Phys.* **2005**, *7*, 2324.
- (18) Hodges, M. P.; Wales, D. J. *Chem. Phys. Lett.* **2000**, *324*, 279.
- (19) Wei, D. Q.; Salahub, D. R. *J. Chem. Phys.* **1997**, *106*, 6086.
- (20) Schmitt, U. W.; Voth, G. A. *J. Chem. Phys.* **1999**, *111*, 9361.
- (21) Li, Z. Q.; Scheraga, H. A. Monte-Carlo-minimization approach to the multiple-minima problem in protein folding. *Proceedings of the National Academy of Sciences of the United States of America*; National Academy of Sciences of the United States of America: Washington, DC, 1987.
- (22) Wales, D. J.; Hodges, M. P. *Chem. Phys. Lett.* **1998**, *286*, 65.
- (23) Swendsen, R. H.; Wang, J. S. *Phys. Rev. Lett.* **1986**, *57*, 2607.
- (24) Earl, D. J.; Deem, M. W. *Phys. Chem. Chem. Phys.* **2005**, *7*, 3910.
- (25) James, T.; Wales, D. J. *J. Chem. Phys.* **2005**, *122*, 134306.
- (26) Nakayama, A.; Seki, N.; Taketsugu, T. *J. Chem. Phys.* **2009**, *130*, 024107.
- (27) Iyengar, S. S.; Day, T. J. F.; Voth, G. A. *Int. J. Mass Spectrom.* **2005**, *241*, 197.
- (28) Termath, V.; Sauer, J. *Mol. Phys.* **1997**, *91*, 963.
- (29) Li, X. H.; Teige, V. E.; Iyengar, S. S. *J. Phys. Chem. A* **2007**, *111*, 4815.
- (30) Stillinger, F. H.; Weber, T. A. *Phys. Rev. A* **1982**, *25*, 978.
- (31) Stillinger, F. H.; Weber, T. A. *Science* **1984**, *225*, 983.
- (32) Wales, D. J. *Mol. Phys.* **1993**, *78*, 151.
- (33) Calvo, F.; Doye, J. P. K.; Wales, D. J. *Chem. Phys. Lett.* **2002**, *366*, 176.
- (34) Wales, D. J. Properties of Landscape. In *Energy Landscape*, 1st ed.; Saykally, R., Zewail, A., King, D., Eds.; Cambridge University Press: Cambridge, U. K., 2003; Vol. 1, p 364.
- (35) Sharapov, V. A.; Meluzzi, D.; Mandelshtam, V. A. *Phys. Rev. Lett.* **2007**, *98*.
- (36) Nguyen, Q. C.; Ong, Y. S.; Soh, H.; Kuo, J. L. *J. Phys. Chem. A* **2008**, *112*, 6257.
- (37) Ong, Y. S.; Keane, A. J. *IEEE Trans. Evol. Comput.* **2004**, *8*, 99.
- (38) Turner, G. W.; Tedesco, E.; Harris, K. D. M.; Johnston, R. L.; Kariuki, B. M. *Chem. Phys. Lett.* **2000**, *321*, 183.
- (39) Ong, Y. S.; Krasnogor, N.; Ishibuchi, H. *IEEE Trans. Syst., Man, Cybernet., Part B: Cybernet.* **2007**, *37*, 2.
- (40) Ballester, P. J.; Richards, W. G. *J. Comput. Chem.* **2007**, *28*, 1711.
- (41) Becke, A. D. *Phys. Rev. A* **1988**, *38*, 3098.
- (42) Lee, C.; Yang, W.; Parr, R. G. *Phys. Rev. B* **1988**, *37*, 785.
- (43) Frisch, M. J.; Trucks, G. W.; Schlegel, H. B.; Scuseria, G. E.; Robb, M. A.; Cheeseman, J. R.; Montgomery, J. A., Jr.; Vreven, T.; Kudin, K. N.; Burant, J. C.; Millam, J. M.; Iyengar, S. S.; Tomasi, J.; Barone, V.; Mennucci, B.; Cossi, M.; Scalmani, G.; Rega, N.; Petersson, G. A.; Nakatsuji, H.; Hada, M.; Ehara, M.; Toyota, K.; Fukuda, R.; Hasegawa, J.;

- Ishida, M.; Nakajima, T.; Honda, Y.; Kitao, O.; Nakai, H.; Klene, M.; Li, X.; Knox, J. E.; Hratchian, H. P.; Cross, J. B.; Bakken, V.; Adamo, C.; Jaramillo, J.; Gomperts, R.; Stratmann, R. E.; Yazayev, O.; Austin, A. J.; Cammi, R.; Pomelli, C.; Ochterski, J. W.; Ayala, P. Y.; Morokuma, K.; Voth, G. A.; Salvador, P.; Dannenberg, J. J.; Zakrzewski, V. G.; Dapprich, S.; Daniels, A. D.; Strain, M. C.; Farkas, O.; Malick, D. K.; Rabuck, A. D.; Raghavachari, K.; Foresman, J. B.; Ortiz, J. V.; Cui, Q.; Baboul, A. G.; Clifford, S.; Cioslowski, J.; Stefanov, B. B.; Liu, G.; Liashenko, A.; Piskorz, P.; Komaromi, I.; Martin, R. L.; Fox, D. J.; Keith, T.; Al-Laham, M. A.; Peng, C. Y.; Nanayakkara, A.; Challacombe, M.; Gill, P. M. W.; Johnson, B.; Chen, W.; Wong, M. W.; Gonzalez, C.; Pople, J. A. *Gaussian 03*, revision D.01; Gaussian, Inc.: Pittsburgh, PA, 2004.
- (44) Stillinger, F. H. *Phys. Rev. E* **1999**, *59*, 48.
- (45) Wales, D. J.; Doye, J. P. K. *J. Chem. Phys.* **2003**, *119*, 12409.
- (46) Bogdan, T. V.; Wales, D. J.; Calvo, F. *J. Chem. Phys.* **2006**, *124*, 1.
- (47) Lovejoy, E. R.; Bianco, R. *J. Phys. Chem. A* **2000**, *104*, 10280.
- (48) Wang, Y.-S.; Chang, H.-C.; Jiang, J.-C.; Lin, S. H.; Lee, Y. T.; Chang, H.-C. *J. Am. Chem. Soc.* **1998**, *120*, 8777.

CT900123D